International Journal of Thermophysics, Vol. 19, No. 2, 1998

Pyroelectric Thermal-Wave Resonant Cavity: A Precision Thermal Diffusivity Sensor for Gases and Vapors[1]

J. Shen,[2] A. Mandelis,[2, 3] and T. Ashe[4]

A novel thermal-wave resonant cavity (TWRC) was constructed and used for thermophysical measurements of gases and vapors, with an AC current-heated thin-film resistive element acting as a thermal-wave source. A thin-film pyroelectric element was used both as a cavity wall and as a signal transducer. A theoretical model of the cavity length-scanned thermal-wave field was developed to quantify the standing-wave resonance antinode patterns in the demodulated lock-in signal output in-phase and quadrature channels. These resonance extrema were used to measure precisely the thermal diffusivity of the intracavity gas or vapor. Seven high-purity gases (nitrogen, dry air, oxygen, methane, hydrogen in nitrogen, pure hydrogen, and helium) were measured using the cavity. Fourth-significant-figure precision was obtained for this parameter, with standard deviations less than 0.32% for the five measurements performed with each gas. Furthermore, three grades of gasoline vapors from Imperial Oil were studied with the cavity. The measured thermal diffusivities showed that the TWRC can monitor fundamental evaporation kinetics as an analytical quality-control instrument. These results, together with the simplicity of TWRC sensor fabrication, are indicative of its potential to become a new standard measurement instrument for the determination of gas thermal diffusivity with improved precision, and a new *in situ* monitor of chemical evaporation kinetics over conventional methodologies, such as gas chromatography and mass spectrometry.

KEY WORDS: gasoline; hydrocarbons; kinetic measurements; resonance; sensor; standing waves; thermal diffusivity; thermal wave.

[1] Invited paper presented at the Thirteenth Symposium on Thermophysical Properties, June 22–27, 1997, Boulder, Colorado, U.S.A.

[2] Photothermal and Optoelectronic Diagnostics Laboratories, Department of Mechanical and Industrial Engineering, University of Toronto, Toronto, Ontario M5S 3G8, Canada.

[3] To whom correspondence should be addressed.

[4] Research Department, Imperial Oil, P.O. Box 3022, Sarnia N7T 7M1, Canada.

0195-928X/98/0300-0579$15.00/0

1. INTRODUCTION

The thermal-wave resonant cavity (TWRC) has been introduced [1] and successfully used [2] to measure the thermal diffusivity of room air by monitoring the spatial behavior of in-cavity thermal waves. In its original design, the cavity consisted of two walls. A very thin aluminum-film wall, exposed to a modulated laser at a preset audio frequency, f, produced an AC thermal source at that modulation frequency. The source acts as a surface heat-flux generator and conductively launches alternating periodic heating and cooling cycles in the gaseous medium above it ("a thermal wave"). When another wall, which is also a thermal-to-electrical energy transducer, such as a pyroelectric thin film (polyvinylidene fluoride; PVDF), is placed parallel to the thermal-source wall and across the gap at a distance L, this transducer generates an oscillating electrical signal proportional to the amplitude of the pseudo-traveling thermal wave within the cavity at the position of the transducer. There is also phase information in that signal, regarding the delay of the thermal oscillation at that position compared with the modulated surface source oscillation. The pyroelectric signal from the PVDF, or some other solid-state pyroelectric crystal, is then demodulated with a lock-in amplifier to gate out unwanted background noise and maximize the signal-to-noise ratio (SNR), at the reference frequency f. It has been discovered [1, 2] that there are standing-wave patterns in both the lock-in in-phase and the quadrature channels, very much like the pressure waves in an acoustic tube (or music pipe). The major difference here is the diffusive nature of thermal conduction (a spatially damped "pseudo-propagating" wave), which manifests itself as an amplitude envelope exponentially decaying into the gas medium above the surface thermal-wave source. Furthermore, the cavity length, L, can be scanned with a micrometer stage, so as to allow "tuning" of the cavity to the principal antinode (resonance) of the standing thermal-wave pattern. Typical cavity lengths are in the 250-μm to 3-mm range. This operation turns the thermal-wave cavity into a resonator, with a very high (exponential) sensitivity to the thermal power transport property, i.e., the thermal diffusivity α_g of the intracavity medium. Therefore, this device can yield measurements of this thermophysical property of the gaseous medium with very high precision.

In its original inception, the TWRC used a laser and an aluminum thin-film optical-to-thermal energy converter to generate thermal waves. To reduce the cost and volume of the device, as well as to make it portable and rugged, the TWRC was redesigned for this work: Instead of the laser and aluminum foil, a thin-film resistive element was used, through which an AC current can be passed at a frequency f. The Joule heating effect in

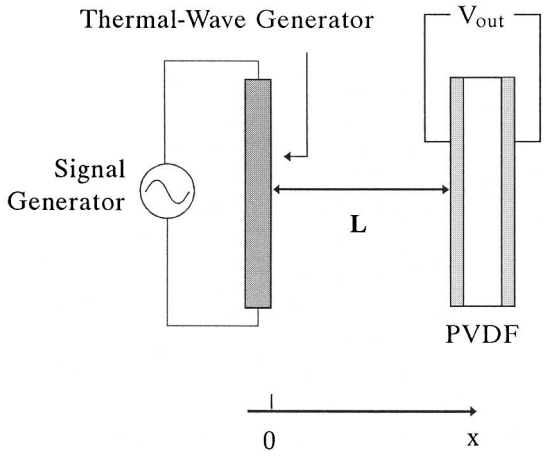

Fig. 1. A schematic diagram of the thermal-wave resonant cavity sensor.

the resistive film acts as an AC thermal-wave source, which is labeled "thermal-wave generator" (TWG) in Fig. 1. In this work, the thermal diffusivity-value resolution of the new setup was tested by measuring the TWRC signal with various intracavity gases of high purity, as well as with various grades of gasoline vapor. The data were fitted to a theoretical model and the values of the thermal diffusivities were extracted.

2. THEORY

Figure 1 is a schematic diagram of the thermal-wave resonant cavity. Assuming that thermal radiation and convection are negligible (a valid assumption only at low-source thermal-wave amplitudes) and the PVDF is thermally thick and thus may be treated as semiinfinite [3], the one-dimensional thermal conduction processes in the geometry of Fig. 1 can be expressed as [3–5]

$$\frac{d^2T_g}{dx^2} - \sigma_g^2 T_g = 0, \qquad 0 \leqslant x \leqslant L \tag{1a}$$

$$\frac{d^2T_p}{dx^2} - \sigma_p^2 T_p = 0, \qquad L \leqslant x \tag{1b}$$

Here

$$\sigma_j \equiv (1+i)\sqrt{\frac{\pi f}{\alpha_j}} \tag{2}$$

is the complex thermal diffusion coefficient and T_j is the complex temperature in material j with thermal diffusivity α_j ($j=$ g and p, referring to the gas and pyroelectric PVDF, respectively). L is the distance between the thermal-wave generator and the PVDF detector (the TWRC length). The bounded solutions of Eqs. (1) are

$$T_g = C_1 e^{-\sigma_g x} + C_2 e^{\sigma_g x} \qquad 0 \leqslant x \leqslant L \tag{3a}$$

$$T_p = C_3 e^{-\sigma_p (x-L)} \qquad L \leqslant x \tag{3b}$$

The coefficients, C_1 to C_3, can be determined by boundary conditions of temperature and heat flux continuity at $x=L$ and by

$$T = T_0, \qquad x = 0 \tag{4}$$

The T_0 in Eq. (4) is the temperature amplitude of the thermal-wave generator. After some algebraic manipulations, one obtains

$$C_3 = \frac{2T_0 b_{gp} \exp(-\sigma_g L)}{(1+b_{gp}) - (1-b_{gp}) \exp(-2\sigma_g L)} \tag{5}$$

For the semiinfinite, thermally thick PVDF film ($\sigma_p L_p \gg 1$, where L_p is the thickness of the PVDF film), the pyroelectric (PE) voltage response is [5]

$$V(f) = S(f) \frac{C_3}{\sigma_p} \tag{6}$$

where $S(f)$ is an instrumental factor, which is constant for a particular frequency. Finally, the PE voltage is proportional to the thermal-wave intensity at the position of the PVDF transducer ($x=L$) and can be expressed as follows:

$$V(f, L) = \frac{2T_0 S(f)\, b_{gp} \sigma_p^{-1} \exp(-\sigma_g L)}{(1+b_{gp}) - (1-b_{gp}) \exp(-2\sigma_g L)} \tag{7}$$

In Eqs. (5) and (7),

$$b_{gp} = \frac{K_g \sqrt{\alpha_p}}{K_p \sqrt{\alpha_g}} \tag{8}$$

is the thermal coupling coefficient at the interface between the gas and the PVDF detector. K_g and K_p denote the thermal conductivity of the gas and PVDF, respectively. The real part of Eq. (7), $\mathrm{Re}[V(f, L)]$, stands for the demodulated signal in the lock-in in-phase (IP) channel, whereas the imaginary part, $\mathrm{Im}[V(f, L)]$, stands for the signal in the quadrature (Q) channel. Equation (7) shows that the PE signal varies with current modulation frequency f and cavity length L. Length or frequency scans can thus be experimentally conducted to measure the thermal diffusivity of the gas within the cavity. It has been established that the cavity-length scan produces more precise results of higher SNR; in addition, it is simpler and easier to carry out [1, 2]. Therefore, only length-scan experiments were performed with the new TWRC setup.

3. EXPERIMENTAL PROCEDURE

The TWG in Fig. 1 is activated by an AC signal generator; a PVDF circular film, 52 μm thick and 0.8 cm in diameter, is enclosed in an Inficon housing and acts as a thermal-wave signal transducer. The PE signal from the PVDF is then amplified by a preamplifier (ITHACO Model 1201), as shown in Fig. 2, and its output is fed into a lock-in amplifier (EG&G Model 5204). The TWG is mounted on a micrometer stage, allowing the cavity length to vary as desired by a step motor controlling the micrometer stage of 10-μm resolution. The data acquisition is facilitated by a personal computer connected to the lock-in amplifier through an analog-to-digital converter. The TWRC is placed in an enclosed cell which provides a controlled environment to measure the values of thermal diffusivity of the intracavity gas or vapor.

This new experimental setup was used to measure pyroelectrically the thermal diffusivity of highly pure gases from Matheson, Canada. These gases were nitrogen (99.998%), air (Ultra Zero), oxygen (99.8%), methane (99.97%), (1.05 ± 0.02%) hydrogen in nitrogen, hydrogen (99.9995%), and helium (99.995). During a measurement, the TWG varies from 0.25 to 3.00 mm, and at every particular position, the PE signal is sampled 10 times and averaged. A signal (amplitude and phase, or IP and Q) profile curve as a function of cavity length is thus obtained. For each gas, five measurements were made, and the experimental data were fitted (in the least-squares sense) to the foregoing theoretical model of the PE signal,

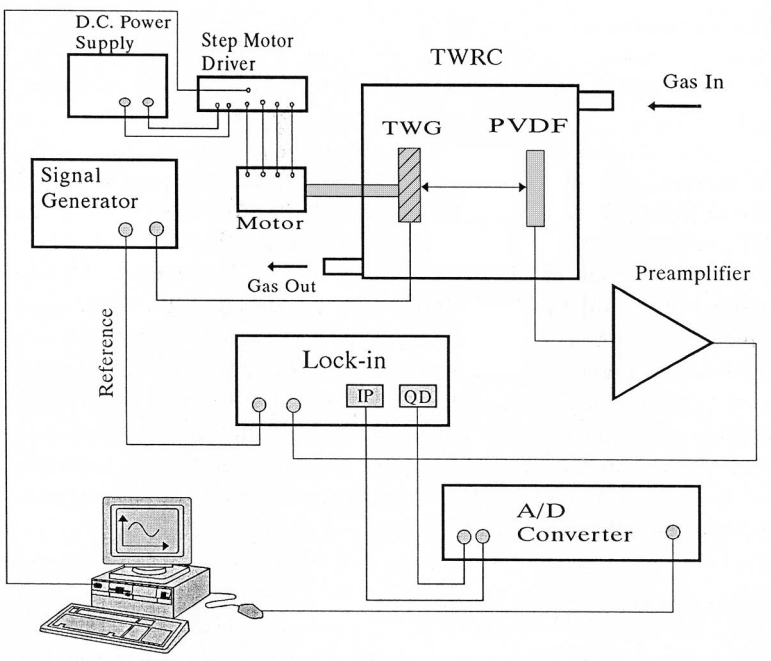

Fig. 2. Block diagram of the experimental system.

with the gas thermal diffusivity being the best-fit parameter. The thermal diffusivity value for each measurement was calculated in this manner. The five thermal diffusivity values were then averaged and recorded as the mean value of the gas, along with the standard deviation.

Applications of the TWRC to distinguish among various grades of gasoline by measuring their thermal diffusivity values were also conducted. A small amount (about 5 ml) of the sample of each gasoline was placed inside the enclosed cell. After the signal level reached the steady state, the vapor thermal diffusivity was measured five times and averaged. The gasoline samples were obtained from Imperial Oil Ltd., Canada. They were labeled IOP11572 (Super 94), IOP11574 (Extra 89), and IOP11573 (Rul 87). HPLC-grade *n*-pentane (from Fisher Scientific, Canada) was also measured, as the gas chromatographic (GC) analysis data supplied by Imperial Oil's Research Department showed that pentanes were one of the main chemical components of the gasoline samples.

In the experiments attention was paid to the excitation current intensity of the TWG, which should be low enough to ensure that conduction is the dominant heat transfer power mode, and radiation heat transfer from the TWG to the pyroelectric detector is negligible. The threshold for the

latter mechanism can be found by monitoring the change in the thermal diffusivity value of a particular gas as a function of the source current peak-to-peak value: the calculated thermal diffusivity increases with increasing current amplitude if direct thermal radiation from the TWG is important. When the current is low enough, the thermal diffusivity does not change with increasing current amplitude. We conducted our experiments in this source current region.

4. RESULTS AND DISCUSSION

4.1. Resonance Patterns

Heat transfer inside the TWRC obeys Fourier's law [4]:

$$-K\nabla T(\mathbf{r}, t) = \mathbf{F}(\mathbf{r}, t) \tag{9}$$

where $\mathbf{F}$ is the spatially and temporally varying heat flux. In the case of thermal-wave excitation the time-modulated component of $\mathbf{F}$ is $\exp(i\omega t)$, and the amplitude of the oscillation decays exponentially from source to detector within the cavity with an almost-linear phase shift, as shown in Fig. 3. However, the PE signals in both the IP and the Q channels exhibit

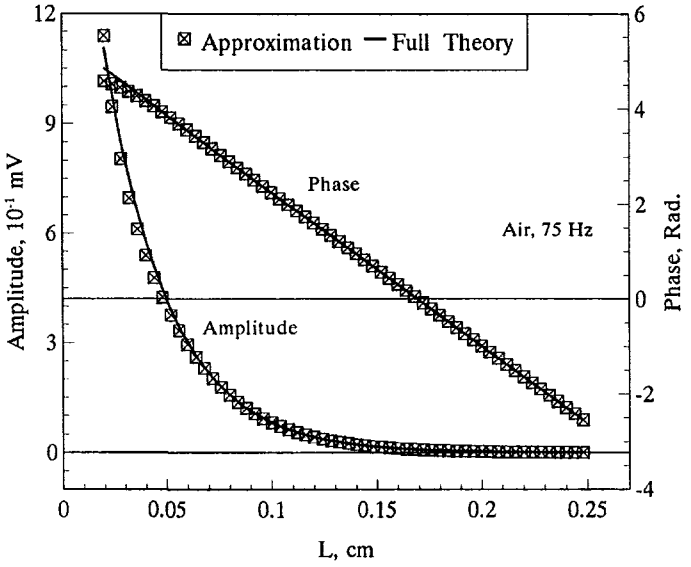

Fig. 3. Theoretical curves of amplitude and phase versus thermal-wave resonant cavity length L with $\alpha_g = 2.214 \times 10^{-5}\ \mathrm{m^2 \cdot s^{-1}}$ at frequency $f = 75$ Hz.

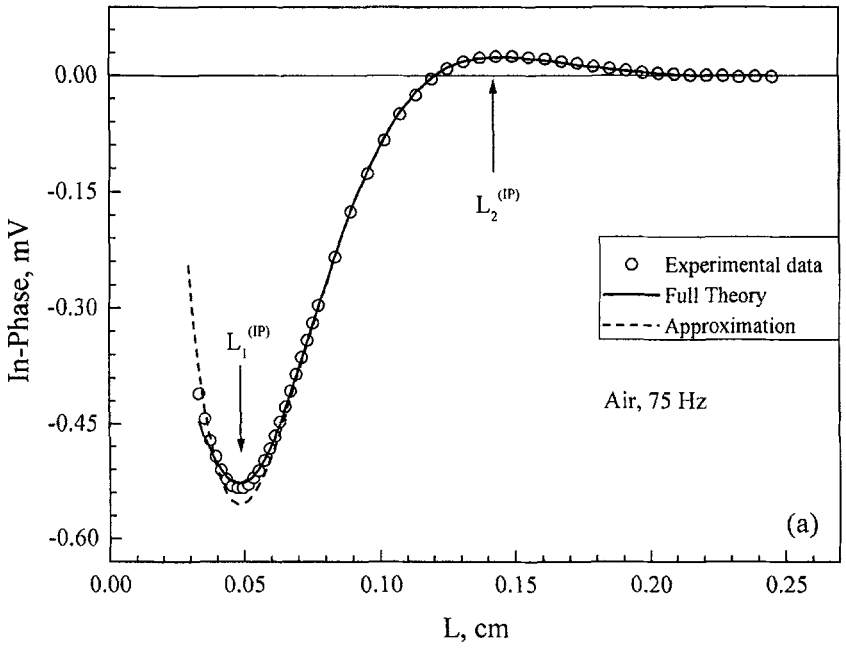

Fig. 4. Experimental and theoretical curves versus thermal-wave resonant cavity length L at $f = 75$ Hz with a single-parameter (thermal diffusivity) fit. The value $\alpha_g = 2.214 \times 10^{-5}\ m^2 \cdot s^{-1}$ at $T = 298$ K was found by the best fit for air. (a) In-phase signal; (b) quadrature signal.

resonant standing-wave patterns shown in Figs. 4a and 4b. It can be proven [1] that the resonance extrema (antinodes) occur at positions

$$L_1^{(IP)} = \tfrac{1}{4}\lambda_g, \qquad L_1^{(Q)} = \tfrac{1}{2}\lambda_g, \qquad L_2^{(IP)} = \tfrac{3}{4}\lambda_g \tag{10}$$

Here

$$\lambda_g = 2\sqrt{\pi\alpha_g/f} \tag{11}$$

is the thermal wavelength in the intracavity gas medium. The relevant parameters of PVDF and air are [3, 6]: $K_p = 0.13\ W \cdot m^{-1} \cdot K^{-1}$, $\alpha_p = 5.4 \times 10^{-8}\ m^2 \cdot s^{-1}$, $K_g = 2.624 \times 10^{-2}\ W \cdot m^{-1} \cdot K^{-1}$, and $\alpha_g = 2.216 \times 10^{-5}\ m^2 \cdot s^{-1}$. Inserting these values in Eq. (8) one obtains $b_{gp} = 9.96 \times 10^{-3} \ll 1$. For hydrogen gas, the thermal diffusivity of which is much larger than that of air [6], $K_g = 0.182\ W \cdot m^{-1} \cdot K^{-1}$ and $\alpha_g = 1.554 \times 10^{-4}\ m^2 \cdot s^{-1}$. Then $b_{gp} = 2.61 \times 10^{-2}$, which is still much smaller than 1 and therefore negligible compared to unity in the denominator of Eq. (7),

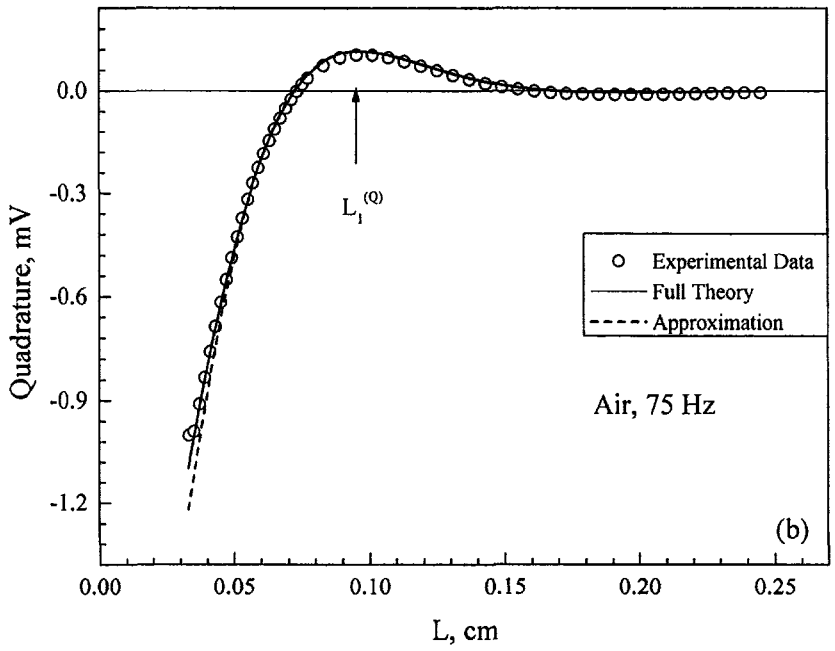

Fig. 4. (*Continued*)

the expression for the PE output voltage. When L is large enough, $\exp(-2\,|\sigma_g|\,L) \ll 1$. Therefore, Eq. (7) becomes

$$V_{\text{approx}}(f) = 2T_0 S(f)\, b_{gp} \sigma_p^{-1} \exp(-\sigma_g L) \tag{12}$$

When f is fixed, the real and imaginary parts of Eq. (12) yield

$$\text{IP}_{\text{approx}} \propto \frac{\exp(-a_g L)}{a_p} [\cos(a_g L) - \sin(a_g L)] \tag{13}$$

$$\text{Q}_{\text{approx}} \propto -\frac{\exp(-a_g L)}{a_p} [\cos(a_g L) + \sin(a_g L)] \tag{14}$$

Here

$$a_j = \sqrt{\frac{\pi f}{\alpha_j}} \tag{15}$$

When

$$a_g L_n^{(IP)} = (n - \tfrac{1}{2})\,\pi, \qquad n = 1, 2, 3,... \tag{16}$$

the in-phase signal is an antinode in the standing thermal-wave pattern. $L_n^{(IP)}$ is the nth extremum in the in-phase channel and is equal to

$$L_n^{(IP)} = (n - \tfrac{1}{2})\,\frac{\lambda_g}{2}, \qquad n = 1, 2, 3,... \tag{17}$$

When n is odd, the extrema are negative, and when n is even, the extrema are positive. Similarly, when

$$a_g L_n^{(Q)} = n\pi, \qquad n = 1, 2, 3,... \tag{18}$$

or, equivalently, when

$$L_n^{(Q)} = \frac{n}{2}\,\lambda_g, \qquad n = 1, 2, 3,... \tag{19}$$

the quadrature signal is an antinode. $L_n^{(Q)}$ is the nth extremum of the quadrature channel. Figure 4 shows the in-phase and quadrature signals of Eqs. (7) and (12), i.e., the full and approximate calculations. Differences between these two calculations occur, as expected, near the origin, where L is small and does not satisfy the approximation condition, $\exp(-2\,|\sigma_g|\,L) \ll 1$. Physically, it is in this region where the effect of multiple "interreflections" of the thermal wavefronts between the two cavity walls is most pronounced to affect the spatial distribution of the standing wave pattern. However, the positions of the extrema of either IP and Q signals are not affected by the approximation Eq. (12). Numerical calculation with the exact expression, Eq. (7), confirms this observation, as shown in Table I. The exact positions of the extrema in air are very close to those predicted also by the

Table I. Numerical Calculation of the TWRC Extremum Positions in Air Using Eq. (7).

f (Hz)	λ_g (cm)	$L_1^{(IP)}/\lambda_g$	$L_1^{(Q)}/\lambda_g$	$L_2^{(IP)}/\lambda_g$
10.00	0.5307	0.2500	0.5000	0.7499
50.00	0.2373	0.2500	0.5000	0.7499
100.0	0.1678	0.2499	0.4999	0.7500
150.0	0.1370	0.2500	0.4999	0.7499
200.0	0.1187	0.2499	0.5000	0.7499
300.0	0.09689	0.2499	0.4999	0.7499

approximate Eqs. (17) and (19) for several frequencies. Therefore, the approximate extremum positions in Eqs. (17) and (19) can be used for accurate, quick, and easy calculations of the thermal diffusivity of the intracavity gas [1, 2], without recourse to the full (and more complicated) expression, Eq. (7).

4.2. Static Thermophysical Measurements of High-Purity Gases

There are two ways of calculating a gas-phase thermal diffusivity value from the experimental data: by using the extrema positions or directly by fitting the exact theoretical Eq. (7) to the experimental data. To determine precisely the positions of the exrema, 11th-order numerical polynomial fits to the experimental data were used to obtain an equation describing the experimental curve. With this equation, the positions of the exrema could be precisely determined, and the gas thermal diffusivity could be deduced. In the experiment, one should carefully choose the modulation frequency in order to get a sharp resonant peak (actually a trough), which is necessary for precise diffusivity determinations. If the frequency is too low, the signal is strong, but the peak is too flat for precise determination of its maximum; if the frequency is too high, the peak is quite sharp, but the signal-to-noise ratio is compromised, which makes identification of the peak position difficult. We chose 75 Hz as the operating frequency to measure nitrogen, air, oxygen, methane, and ($1.05 \pm 0.02\%$) hydrogen in nitrogen and 500 Hz for measuring hydrogen and helium.

Figure 4 shows a set of typical experimental data of air and their best fit. The full theory, Eq. (7), fits the data very well, with a correlation coefficient of $R > 0.9999$. Using the best-fit method, we determined the thermal diffusivity value of air to be $2.214 \times 10^{-5}\ m^2 \cdot s^{-1}$, while the extremum-position determination method gave $2.225 \times 10^{-5}\ m^2 \cdot s^{-1}$. The relative difference between the two thermal diffusivity values is less than 0.5%. Between these two methods, it was found that the latter is relatively easier to use and less time-consuming. Therefore, the extremum-position determination method was used to calculate the thermal diffusivity values for all gases and vapors. The approximate theory, Eq. (12), could also be fitted to the experimental data with air as the intracavity gas. However, the thermal diffusivity value obtained from this fit was $2.365 \times 10^{-5}\ m^2 \cdot s^{-1}$, which is higher than the foregoing values and higher than the literature values, as shown in Table II.

Table II displays the experimental TWRC results of seven gases at 298 K and compares them with accepted literature values. The high degree of reproducibility of the TWRC method, with standard deviations less than 0.32% of the averaged thermal diffusivity values for five consecutive measurements, should be noted. Overall, the measured thermal diffusivity

Table II. Thermal Diffusivities of Gases Measured with the Thermal-Wave Resonant Cavity Sensor ($T = 298$ K)

Gas	Thermal diffusivity ($\times 10^{-4}$ m$^2 \cdot$ s^{-1})[a]	D, averaged value (%)	Literature value ($\times 10^{-4}$ m$^2 \cdot$ s^{-1}) ($T = 300$ K)
Nitrogen (zero)	0.2186 ± 0.0007	0.320	0.22044[b]
Dry air (ultrazero)	0.2224 ± 0.0007	0.315	0.19,[c] 0.22160,[b] 0.228[d]
Oxygen	0.2246 ± 0.0007	0.312	0.22353[b]
Methane (99.97%)	0.2326 ± 0.0006	0.245	0.234[e]
$(1.05 \pm 0.02\%)$	0.2246 ± 0.0007	0.312	
Hydrogen in nitrogen			
Hydrogen (99.9995%)	$(0.1564 \pm 0.0001) \times 10$	0.0863	1.554[b]
Helium	$(0.1895 \pm 0.0005) \times 10$	0.284	1.875[e]

[a] Averaged value of five measurements.
[b] Quoted from Ref. 6. These probably are not experimentally measured values, as they can be obtained from a calculation with the values of thermal conductivity K_g, density ρ_g, and specific heat c_g of gases in Ref. 6.
[c] Quoted from Ref. 7.
[d] Quoted from Ref. 8.
[e] Calculated using the data in Ref. 9.

values are seen to be in very good agreement with literature values. Fourth-significant-figure precision was obtained in the measured thermal diffusivity value for each gas, which shows that the TWRC thermophysical measurements could be the most precise experimental method to date for determining the thermal diffusivity values of gases. The thermal diffusivity value of methane could not be found in literature. This is probably the first time the thermal diffusivity of methane has been directly measured experimentally. It should be noted that the standard deviations of the diffusivity values for the high thermal conductors H2 and He are among the smallest in the group, despite the fact that the modulation frequency used to produce these measurements is much higher (500 Hz) than that used for the remaining gases (75 Hz). This is the result of the combination of the higher thermal diffusivity producing stronger PE signals *and* the higher modulation frequency giving a more precise definition of the resonant peak.

4.3. Transient and Steady-State Thermophysical Measurements of Gasoline Vapor Samples

Figure 5 shows the evolution of the various transients of the evaporation kinetics of the gasoline samples monitored by the TWRC at a fixed cavity length L near the position of the first in-phase resonance. The IP

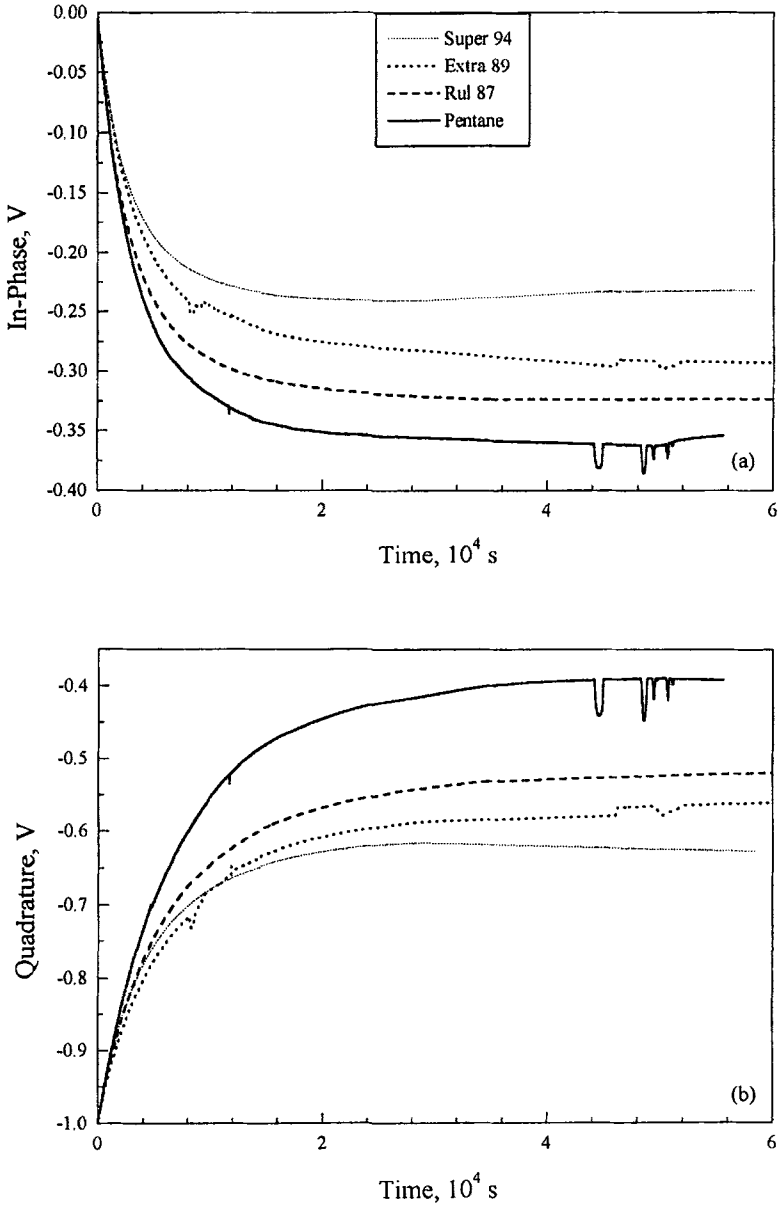

Fig. 5. The evolution of the various transients of the evaporation kinetics of gasoline and pure pentane samples monitored by the TWRC at a fixed cavity length L near the position of the first in-phase resonance.

Table III. Thermal-Diffusivity Values of Gasoline Samples (Samples Within the TWRC; $T = 298$ K)

	Thermal diffusivity ($\times 10^{-4}$ m$^2 \cdot$ s^{-1})[a]		Pentanes in gasoline (wt%)
	First set	Second set	
IOP11572 (Super 94)	0.0738 ± 0.0001	0.0735 ± 0.0002	14.076
IOP11574 (Extra 89)	0.0699 ± 0.0001	0.0697 ± 0.0004	21.524
IOP11573 (Rul 87)	0.0596 ± 0.0001	0.0597 ± 0.0004	33.138
n-pentane	0.0386 ± 0.0002		

[a] Each set consisted of five measurements; $f = 75$ Hz.

signal decay as a function of time is as expected, as the relative spatial density of the high molecular weight vapor molecules of gasoline samples increases in the enclosure volume and inside the intracavity space, thus decreasing the thermal diffusivity of the gas. It can be seen from Fig. 5 that the decay time constants and the final saturated values are different for different gasoline samples. The transient data carry (as yet unquantified) information about the molecular/mass diffusivity, D, of each gasoline vapor in air, through the dependence of this quantity on the thermal diffusivity, $\alpha = \alpha(D)$. The noise superposed on some of the transients is related to the TWRC signal processing instrumentation.

Very reliable and highly precise thermal diffusivity data were obtained for all three gasoline samples examined in this work. These measurements were performed after the signal had reached the steady state, indicating that the entire air mass had been expelled from the enclosure volume and replaced by gasoline vapor. The results are shown in Table III. The concentration of pentanes in these gasoline samples was determined by gas chromatographic (GC) data to be the highest constituent among large numbers of constituent hydrocarbons and other chemicals. The higher-quality gasolines were found to have a higher thermal diffusivity, which may be related to their low pentane concentration. It can be seen from Table III that the thermal diffusivity of gasolines decreases with increasing pentane concentration, consistent with the very low value of diffusivity for this hydrocarbon, as independently measured using *n*-pentane as the intracavity vapor. The various grades of gasoline could thus be distinguished by their thermal diffusivity values, using the TWRC sensor.

5. CONCLUSIONS

A new setup of the thermal-wave resonant cavity has been presented, with a theoretical analysis and experimental applications. The resonance

patterns appear in the demodulated lock-in in-phase and quadrature channels. The first and second extrema of the IP signal are located at cavity lengths equal to one-quarter and three-quarters of the thermal-wave wavelength λ_g, respectively, while the first Q resonance peak is at one-half λ_g. These extremum positions can be used to calculate the thermal diffusivity of the intracavity gas. Seven highly pure gases were measured with the cavity, and very precise thermal diffusivity values were obtained with less than 0.32% variance. This indicates that thermophysical measurements with the TWRC sensor have the potential to become a standard method of determining gas thermal diffusivity values. In addition, the evaporation process of three grades of gasoline were studied using the TWRC sensor, and the thermal diffusivity values of their vapors were measured from the steady-state signals. The results showed that the sensor can be used to distinguish among different grades of gasoline by measuring their vapor thermal diffusivities, instead of the conventional expensive and time-consuming procedures, such as mass spectrometric and gas chromatographic measurements. The analytical potential of the TWRC technique to conduct fundamental kinetic diffusion studies of gasoline and pure hydrocarbons vapor evolution in the cavity was further demonstrated.

ACKNOWLEDGMENTS

The authors are grateful to Imperial Oil Ltd. and the Manufacturing Research Corporation of Ontario for grants, which made this research possible.

REFERENCES

1. J. Shen and A. Mandelis, *Rev. Sci. Instrum.* **66**:4999 (1995).
2. J. Shen, A. Mandelis, and B. D. Aloysius, *Int. J. Thermophys.* **17**:1241 (1996).
3. A. Mandelis and M. M. Zver, *J. Appl. Phys.* **57**:4421 (1985).
4. H. S. Carslaw and J. C. Jaeger, *Conduction of Heat in Solids*, 2nd ed. (Oxford, London, 1959).
5. A. Mandelis, J. Vanniasinkam, S. Budhudu, A. Othonos, and M. Kokta, *Phys. Rev. B* **48**:6808 (1993).
6. J. P. Holman, *Heat Transfer*, 7th ed. (McGraw–Hill, New York, 1990).
7. A. Rosencwaig, *Photoacoustics and Photoacoustic Spectroscopy* (Wiley, New York, 1980), p. 96.
8. Y. S. Touloukian, R. W. Powell, C. Y. Ho, and M. C. Nicolaou, *Thermal Diffusivity* (IFI/Plenum, New York, 1973).
9. D. Lide, *CRC Handbook of Chemistry and Physics*, 75th ed. [Chemical Rubber Co. (CRC), Cleveland, OH, 1994–1995].